Hindawi
International Transactions on Electrical Energy Systems
Volume 2024, Article ID 5536555, 20 pages
https://doi.org/10.1155/2024/5536555

Research Article

Real-Time HIL Simulation of Nonlinear Generalized Model Predictive-Based High-Order SMC for Permanent Magnet Synchronous Machine Drive

Hafidh Djouadi,[1] Kamel Ouari,[1] Youcef Belkhier,[2] and Hocine Lehouche[1]

[1]*Laboratoire de Technologie Industrielle et de l'Information (LTII), Faculté de Technologie, Université de Bejaia, Bejaia 06000, Algeria*
[2]*Institut de Recherche de l'Ecole Navale (EA 3634, IRENav), French Naval Academy, Brest 29240, France*

Correspondence should be addressed to Youcef Belkhier; youcef.belkhier@ecole-navale.fr

Received 10 August 2023; Revised 25 September 2023; Accepted 28 February 2024; Published 7 March 2024

Academic Editor: Shaofeng Lu

The dynamics of the permanent magnet synchronous motor (PMSM) are described by nonlinear equations, which present challenges. Variations in external factors such as unidentified disturbances (loads) and evolving motor properties add complexity to control efforts. To tackle these intricacies and limitations, a nonlinear control approach is essential. Recent attention has turned to employing predictive control techniques for nonlinear multivariable systems, offering an intriguing avenue for research. In this context, this study introduces a novel hybrid control approach that addresses nonlinearity, parametric fluctuations, and external disturbances. The method combines two essential components: first, the outer loop utilizes high-order sliding mode control (HSMC) to optimize torque and trajectory speed, mitigating chattering phenomena while preserving the PMSM's convergence and robustness traits. The inner loop, known as the current control, employs the newly developed nonlinear robust generalized predictive control (RNGPC) technique. Importantly, this strategy circumvents the need for direct measurement and observation of external disturbances and parameter uncertainties. The proposed strategy follows a two-phase process. Initially, the reference quadratic current is designed using the electromagnetic torque computed via HSMC, subsequently determining the necessary current to achieve the desired torque. The second phase involves computing the controller law through the robust generalized nonlinear predictive control technique. The approach's strength lies in its ability to maintain stability and convergence in the face of external disturbances and parameter fluctuations, without necessitating precise measurements or knowledge of the disturbances. To validate the proposed control approach, simulation and experimental tests have been conducted across various operational scenarios. The obtained results demonstrate the method's robustness against external disturbances and parameter changes while ensuring rapid convergence and reliable performance.

1. Introduction

In the modern industrial world, permanent magnet synchronous motors (PMSMs) play a significant position in the regulation of processes, automation systems, and the development of renewable energy sources [1]. All of this is attributable to their superior performance in terms of efficiency, torque, and power density as well as their dependability and reduced bulk. In addition, their construction is simpler because they lack mechanical switches, which extends their lifespan and reduces the need for ongoing maintenance [1, 2]. Additionally, these engines have the benefit of releasing zero greenhouse emissions, which is particularly advantageous for environmental conservation [3]. The PMSM, on the other hand, operates like a nonlinear system with quick dynamics, variable operating parameters, and unidentified disturbances [4, 5]. The machine's control is made more difficult by these features. Numerous studies on the control of PMSM have been published in the literature and the business sector as solutions to the

aforementioned issues. The current research indicates that the controls based on linear and nonlinear techniques are controls that are both highly common and useful.

The widely utilized proportional-integral (PI) control is a linear control technique. It generates a continuous reference output, which subsequently undergoes conversion into a digital format via pulse width modulation (PWM)—a fundamental control strategy. Yet, when striving for heightened performance and precision in speed regulation, PI controllers fall short. Alternative methods gaining popularity include state feedback control [6] and impulse control [7]. Remarkably, these approaches share a common requirement: the integration of PWM. Conventional linear control system design typically assumes operation within a linear region. However, the complexities and constraints within power electronics and drive systems, often unreported, introduce numerous limitations and nonlinearities [8]. Such traditional control paradigms might prove insufficient for systems featuring nonlinearity or variable parameters. Their susceptibility to fragility becomes pronounced, especially when stringent demands for accuracy and dynamic system attributes are at play. Consequently, the need arises for control strategies capable of resilience against parameter variations, disturbances, and nonlinearities.

Many methods have been tried to account for the permanent magnet synchronous machine's nonlinearities. In [9], direct control of the speed associated with a state-dependent Riccati equation is described; two explicit limitations are the field-weakening curve and the current amplitude. The cost function at the controller arrival is known, and the problem is, therefore, formulated as a quadratic program with a quadratic constraint. A new extended state observer using sliding mode is proposed in [10] to enhance the disturbance compensation and rejection as well as the dynamical efficiency of PMSM control systems. For a more precise comparison, an extended observer that is based on the fast terminal sliding mode control strategy is described. It has the benefit of greater robustness against load disturbances, finite time integration, and a considerable reduction of the "chattering" phenomenon. An improved nonlinear flux observer is put forth in [11]. Studying the method of rotor position estimate from flux monitoring comes first. The limitations of classic rotor flux variation estimation methods are then investigated, including classical integrator saturation, low-pass filter amplitude decreasing, and phase change. A fuzzy adaptive controller is provided in [12]. The Takagi–Sugeno fuzzy membership criterion allows you to convert the nonlinear PMSM model into equivalent linear submodels. Then, in collaboration with a fractional sliding surface that has an integral criterion, an adaptive controller is developed in order to regulate the PMSM. The authors of [13] expose a sliding mode control (SMC) based on an adaptive speed controller. Using a nonlinear disturbance observer (DO), the hybrid controller SMC is constructed in [14]. The most effective strategy for enhancing the drive systems' ability to reject disturbances is DO-based control. Its performance in dynamic control and load torque disturbance rejection capabilities is weak in the middle. As a result, although the sliding mode occasionally results in high-frequency shifts (chattering), these switches instead produce unwanted behaviors that have the potential to destabilize, harm, or even destroy the system under consideration. Another control strategy that is applied to PMSM control called the "passivity-based control (PBC)" strategy emerges as a distinctive approach that takes into account the intricate interplay between the motor's electrical and mechanical components, subject to specific conditions [1]. PBC manifests in several variants, such as passivity-based current control [15], voltage control [16], and interconnection and damping assignment PBC [17], each catering to precise control objectives within the PMSM system. Moreover, recent strides in PMSM control have introduced pioneering methodologies to elevate performance and resilience. For instance, a robust backstepping compensator, coupled with a nonlinear disturbance observer, fortifies the system against disturbances [18]. This compensator offers improved disturbance rejection capabilities, bolstering the motor's stability and robustness in the presence of external perturbations. Additionally, sensorless control strategies built upon a nonlinear flux observer [19] have gained prominence. These sensorless techniques enable accurate estimation of crucial rotor parameters, such as position and speed, without the need for additional sensors. While these advancements hold promise for simplifying system design and reducing hardware costs, they are not without their challenges. Implementing robust compensators may require careful tuning, and sensorless techniques are often sensitive to parameter variations and may have limitations in rapidly changing operating conditions. Nonetheless, these pioneering methodologies represent valuable contributions to the field of PMSM control, addressing the need for improved performance and resilience in various applications.

Model predictive control (MPC), presently considered one of the most trustworthy control strategies by many researchers, is garnering a lot of interest due to its straightforward implementation, its capacity for direct management of constraints and nonlinearities of the systems, which guarantees satisfactory system performances [20]. MPC is a feedback control algorithm that makes use of a model to forecast outputs over a given period of time. These forecasts are then used to choose the best control by solving a particular optimization problem while adhering to a predefined constraint (cost function) [21]. The three steps of the MPC approach are the feedback structure, the regressive optimization, and the predictive model.

Many composite algorithms based on MPC have been put out in recent years to improve PMSM control performance due to the rapid development of microcontrollers and advances in MPC research [22, 23]. In [24], a cascaded MPC structure with speed control as the outer loop and current control as the inner loop is presented for the PMSM. The external-loop MPC design incorporates a disturbance model with signal generators for zero-frequency and first-frequency modes to lessen the impact of periodic perturbation brought on by current sensor offset inaccuracies in the velocity regulator of a PMSM. The established torque-ripple models, however, are frequently erroneous and complex [23]. To get a good estimate of the

torque, a hybrid approach employing FCS-MPC with a lookup table is suggested [22]. Duty cycle control [25, 26] and quantitative search [27] are two more enhancements that have been suggested. Many of the aforementioned modifications can lessen current ripple and torque. Additionally, some researchers [28] have put a control strategy that combines MPC and observer forth [29]. The authors of [30] study the use of continuous model-time predictive control (CTMPC) to train a PMSM. The MPC problem with a nonlinear perturbation observer and an unknown load torque is solved by the CTMPC using an expansion of the Taylor series. These tests demonstrate the method's effectiveness. However, it is impossible to see ripples brought on by a mechanical component (such as cogging torque and load oscillations) [31]. The construction of a disturbance observer is not straightforward in the case of a PMSM, which makes the analysis of the closed-loop system extremely difficult [32].

This research introduces an innovative hybrid control approach that capitalizes on high-order sliding mode control (HSMC) to attain optimal torque and trajectory speed for the outer loop. This design choice not only enables effective suppression or elimination of the chattering phenomenon but also preserves the system's convergence and robustness attributes. Complementing this, the inner loop employs the robust generalized nonlinear predictive control technique to manage the current control aspect. The proposed control strategy is designed with a holistic understanding of the complete dynamics of the permanent magnet synchronous motor (PMSM). The development of the nonlinear generalized predictive control law is achieved by fine-tuning a newly formulated cost function. To enhance disturbance mitigation, the controller incorporates an integral action. A noteworthy aspect of this novel method is its inherent capacity to enhance system robustness without necessitating detailed knowledge of external disturbances or uncertainties in system parameters.

In this paper, a new design process of continuous model-time predictive control is studied, and a robust nonlinear generalized predictive control law is formulated by optimizing a new cost function, where integral action is added to the controller to enhance disturbance rejection. This novel control strategy offers an analytical solution for the control of multivariable nonlinear systems, eliminating the need for computationally intensive online calculations. An essential characteristic of this proposed control method is its robustness, as it does not depend on prior knowledge of external disturbances or uncertainties in system parameters to achieve superior performance.

The following succinctly expresses this work's contribution and originality:

(i) New nonlinear generalized model predictive-based high-order sliding mode control for permanent magnet synchronous machine with a new optimized cost function is proposed

(ii) The proposed controller guarantees setpoint tracking performance and robustness against sudden load torque variations (external disturbance) as well as parametric variations and eliminates the effects of disturbances without the need for a disturbance observer making it easy to implement

(iii) Numerous numerical simulations are carried out to demonstrate the suggested technique's resistance to parameter changes and outside disruptions where the simulation results demonstrate the efficiency of this control, which enables the system to maintain its stability in a closed loop

The structure of this document is as follows: Section 2 describes the permanent magnet motor system. The calculation of the classical and proposed control strategy for the PMSM is discussed in Section 3. In Section 4, the simulation tests of the suggested approach are presented. Section 5 depicts the experimental results using OPAL-RT. Section 6 concludes with the key findings.

2. Permanent Magnet Synchronous Motor Dynamic Description

Dynamic modeling of PMSM is an indispensable step for control design engineering. It involves the rigorous formulation of mathematical equations that encapsulate the intricate electromagnetic and mechanical dynamics inherent in PMSM. These models serve as a foundational framework for predictive analysis, affording us the capacity to prognosticate the system's response across a spectrum of operational parameters, such as load variations and diverse control algorithms. The paramount utility of dynamic modeling manifests in its role as an enabling instrument for optimizing motor efficiency, architecting high-fidelity control algorithms, and implementing robust fault detection mechanisms. Nevertheless, confronting the nonlinearities intrinsic to PMSM and iteratively refining parameter estimations remain formidable tasks. In spite of these complexities, dynamic modeling persists as a cornerstone of contemporary electric machines and drives research, propelling the frontier of energy-efficient and fault-tolerant motor systems [33, 34]. Assuming the rotor's position has no effect on the inductance and that the rotor's flux axis is parallel to the machine's d-axis. The mathematical model of the PMSM is constructed by transforming the three-phase variables in the stator reference frame into two-phase variables in the rotor d-q reference frame [6]. In this case, the nonlinear mathematical model of the PMSM is given by

$$\begin{cases} v_d = R_s i_d + L_d \dfrac{di_d}{dt} - P w_r L_q i_q, \\ v_q = R_s i_q + L_q \dfrac{di_q}{dt} + P w_r L_d i_d + P w_r \varphi_f, \\ \dfrac{d}{dt} w_r = \dfrac{1}{J}\left(T_{em} - C_r - f w_r\right), \\ T_{em} = \dfrac{3p}{2}\left(\varphi_f i_q + \left(L_d - L_q\right) i_d i_q\right), \end{cases} \tag{1}$$

where R_s, L_d, and L_q are the stator per phase (Ohm) and direct and quadrature axis stator self-inductances in the rotor reference frame (H), respectively. P is a number of poles-pairs, φ_f is links between armatures flux created by rotor magnets (Wb), and J is the inertia moment (kg.m^2). T_{em} is the electromagnetic torque (N-m), J is the inertia moment (kg.m^2), w_r is mechanical rotor speed (rad/sec), and f represents the coefficient of viscous friction (N.m.s/rad).

The synchronous machine model can be expressed as follows:

$$V_{dq} = R_{dq} i_{dq} + L_{dq} \frac{di_{dq}}{dt} + p w_r \mathfrak{F}\left(L_{dq} i_{dq} + \psi_f\right),$$

$$J \frac{dw_r}{dt} + f w_r = T_{em} - C_r, \tag{2}$$

where $i_{dq} = \begin{bmatrix} i_d \\ i_q \end{bmatrix}$ is the stator currents vector in the dq-frame, $L_{dq} = \begin{bmatrix} L_d & 0 \\ 0 & L_q \end{bmatrix}$ is the stator inductions matrix in dq-frame, $\psi_f = \begin{bmatrix} \varphi_f \\ 0 \end{bmatrix}$ is the flux linkages' vector in the dq-frame, $V_{dq} = \begin{bmatrix} v_d \\ v_q \end{bmatrix}$ is the voltage stator's vector in the dq-frame, $R_{dq} = \begin{bmatrix} R_s & 0 \\ 0 & R_s \end{bmatrix}$ is the stator resistance matrix in the dq-frame, $\mathfrak{F} = \begin{bmatrix} 0 & -1 \\ 1 & 0 \end{bmatrix}$, and T_{em} can be written as follows:

$$T_{em} = \frac{3}{2} p \psi_{dq} \mathfrak{F} i_{dq}, \tag{3}$$

$$\psi_{dq} = \begin{bmatrix} \psi_d \\ \psi_q \end{bmatrix} = \left(L_{dq} i_{dq} + \psi_f\right). \tag{4}$$

The dynamics of the current-controlled PMSM can be reduced to the following model:

$$\dot{\psi}_{dq} + p w_r \mathfrak{F} \psi_{dq} = -R_{dq} i_{dq}, \tag{5}$$

$$J \dot{w_r} + f w_r = \frac{3}{2} p \psi_{dq}^T i_{dq} - C_r, \tag{6}$$

$$T_{em} = \frac{3}{2} p \psi_{dq}^T i_{dq}. \tag{7}$$

3. Design of the Proposed Control Approach

Figure 1 illustrates the computational process of the explored strategy, which has two distinct components: the first phase is to design the reference quadratic current using the electromagnetic torque calculated by the HSMC technique, and the required current is then calculated using the required torque. In the second part, the controller law is calculated using the robust generalized nonlinear predictive control technique.

If the direct current id is zero, PMSM runs at its maximum torque. Then, in light of the relationship (4), the d-q axis desired flux is selected as follows [8]:

$$\psi_d^* = \varphi_f, \tag{8}$$

$$\psi_q^* = L_q i_q^*. \tag{9}$$

The desired torque is determined by the following relationship from equations (4) and (5):

$$T_{em}^* = \frac{3}{2} p \psi_{dq}^{*T} \mathfrak{F} \left(\psi_{dq}^* - \psi_f\right). \tag{10}$$

This results in

$$T_{em}^* = \frac{3}{2} p \varphi_f i_q^*. \tag{11}$$

The desired flux along the quadratic axis q, according to equations (9) and (11), is defined by

$$\psi_q^* = \frac{2L_q}{3p\varphi_f} T_{em}^*. \tag{12}$$

3.1. Calculation of the Desired Torque. According to equation (12), the reference torque is formulated as follows:

$$T_{em}^* = J \frac{dw_r^*}{dt} - f\varepsilon, \tag{13}$$

where $\varepsilon = (w_r^* - w_r)$ represents the speed error between the reference and the PMSM velocity. The appropriate dynamic is to reduce this velocity tracking error as much as possible. According to equation (12), the desired torque T_{em}^* has two drawbacks: the dependence of its convergence on the mechanical parameters of the PMSM (J, f) and it is open loop. To address these issues, in [35], the (f) term was removed and T_{em}^* was calculated by a PID controller. However, the authors mentioned that this strategy still has a drawback with the change of J due to the fixed gains of the PID. To address this drawback, SMC is proposed given its high stability, fast dynamic response, and robustness ability to replace PI loop [36]. However, in reality, the sliding approach results in "chattering," which is a sort of high-switching frequency that leads to unintended dynamics, which can destabilize, deteriorate, or even destruct the

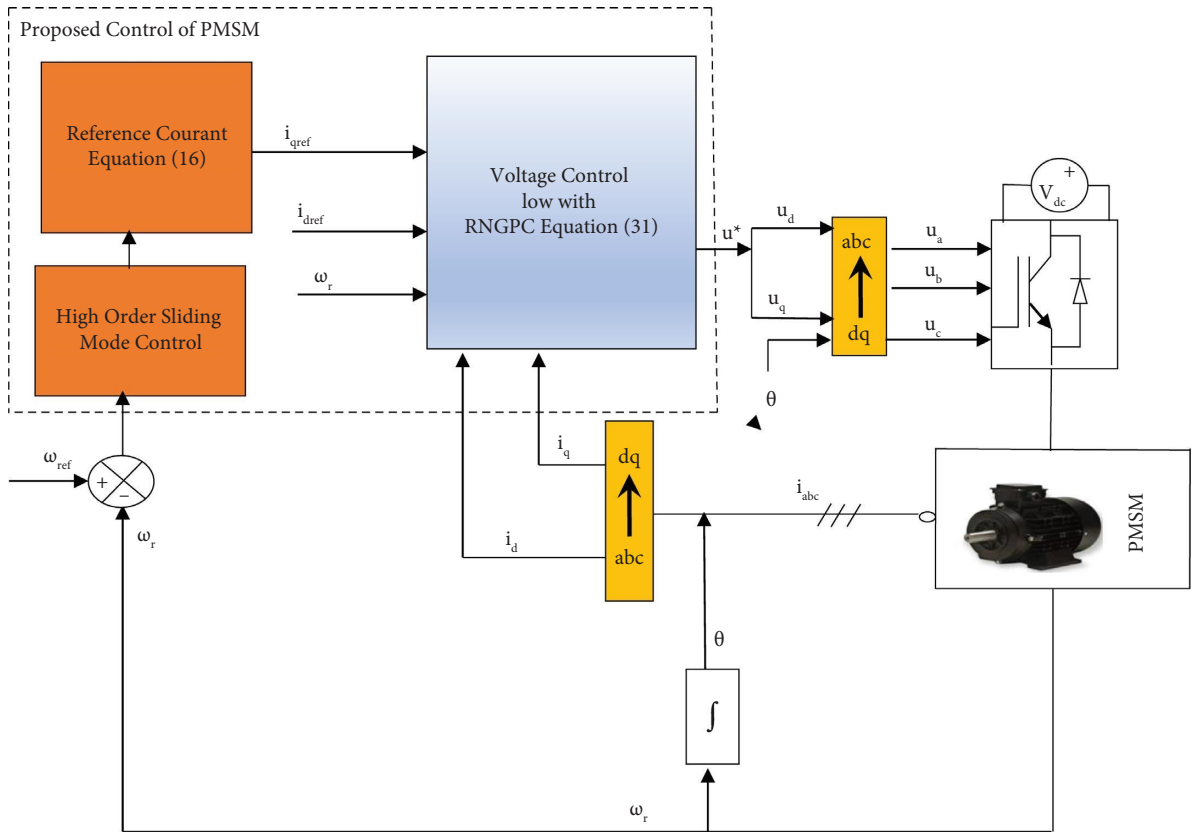

Figure 1: Overall diagram of new proposed strategy HSMC-RNGPC.

system under investigation. To overcome the chattering challenge, a high-order SMC is established, which operates on the assumption of avoiding singularities in the scheme's higher derivatives, in order to overcome the chattering challenge and compensate for the disturbance of the resistive torque in the speed response, and we propose to control the machine using the HSMC strategy to replace the PID and calculate the required torque as shown in the following equation:

$$T_{em}^{*} = J\frac{dw_r^{*}}{dt} - a_1|\varepsilon|^{0.5}\operatorname{sign}(\varepsilon) - a_2\int_0^t \operatorname{sign}(\varepsilon)d\tau, \quad (14)$$

where $a_1 > 0$, $a_2 > 0$, and $\varepsilon = (w_r^{*} - w_r)$ represent the speed error. Referring to a classic cascade control, the input quantity of the system is the reference speed which is compared to the real speed, to generate the setpoint of the transverse component of the current, using the HSMC control law described by the equation (14) and using equation (11), and the setpoint of the transverse component of the current is given by

$$i_q^{*} = \frac{3}{2p\varphi_f}\left(J\frac{dw_r^{*}}{dt} - a_1|\varepsilon|^{0.5}\operatorname{sign}(\varepsilon) - a_2\int_0^t \operatorname{sign}(\varepsilon)d\tau\right). \quad (15)$$

3.2. Model Predictive Control Theory. Model predictive control (MPC) is an advanced control strategy employed in various engineering applications, including the control of permanent magnet synchronous motors (PMSMs). MPC offers a predictive approach to managing the operation of PMSMs by utilizing a dynamic model of the motor system. Here is a detailed explanation of model predictive control in the context of PMSMs: model predictive control starts with a detailed mathematical model of the PMSM, which incorporates the electrical, mechanical, and magnetic dynamics of the motor. This model is used to predict how the motor will behave over a defined prediction horizon into the future. The control objective is to optimize control inputs, typically voltage or current, over this prediction horizon while considering constraints on variables such as current limits, voltage limits, and motor speed. MPC continuously reevaluates and adjusts the control inputs at each control step, ensuring that the system closely follows desired trajectories and minimizes a predefined cost function [35, 36].

One of the key advantages of MPC for PMSM control is its ability to handle complex and nonlinear dynamics, making it suitable for high-performance applications. MPC also accounts for constraints, ensuring that the motor operates safely within its specified limits, which can be crucial in real-world applications. However, MPC does come with some challenges. It requires an accurate dynamic model

of the motor, which may be difficult to obtain in practice due to uncertainties or parameter variations. Additionally, the computational demands of MPC can be significant, especially for high-speed control loops, although advances in hardware and algorithms have helped mitigate this issue. In summary, model predictive control is a powerful strategy for achieving precise and dynamic control of permanent magnet synchronous motors, but its effectiveness depends on the quality of the dynamic model and the computational resources available [37]. For more details about the theory of MPC and its applications, the reader is referred to [38, 39].

The cost function in MPC for PMSMs serves as a cornerstone in achieving optimal motor control. It acts as the guiding criterion for the MPC controller, defining the performance goals and constraints for the system. By formulating a well-designed cost function, engineers can precisely specify the desired trade-offs among various aspects of motor performance, including speed regulation, torque accuracy, energy efficiency, and system stability. Additionally, the cost function plays a crucial role in handling operational constraints, ensuring that control inputs remain within safe limits while striving for optimal performance. MPC's ability to incorporate multiobjective optimization within the cost function enables engineers to balance conflicting goals effectively. Furthermore, the adaptability of the cost function allows MPC to respond to changing operating conditions and disturbances, making it a valuable tool for achieving precise and robust control of PMSMs in diverse applications [40].

3.3. Classical Nonlinear Generalized Predictive Control Design (NGPC). The control approach proposed in this study is based on MPC, and it is currently regarded by many scientists as one of the most reliable control strategies and attracts a lot of attention due to its simple implementation and its ability to directly handle system constraints and nonlinearities, thus ensuring satisfactory system performance [15]. MPC is a feedback control algorithm that uses a model to predict future outputs over a specified period of time, and these predictions are then used to select the optimal control by solving a specific optimization problem while satisfying a predefined constraint (cost function) [16, 24]. The MPC method consists of three steps: the predictive model, the regressive optimization, and the feedback structure. In this paper, the robustness of the classical nonlinear generalized predictive control (NGPC), based on Taylor series expansion, is improved by revising its cost function.

In order to accommodate for the modularization errors and external disturbances comprehensively, the subsequent conditions have been delineated:

$$\begin{cases} R_s = R_s + \Delta R_s, \\ L_d = L_d + \Delta L_d, \\ L_q = L_q + \Delta L_q, \\ \phi_f = \phi_f + \Delta \phi_f, \\ J = J + \Delta J, \\ f = f + \Delta f. \end{cases} \tag{16}$$

The electrical subsystem model for the synchronous machine, considering the influence of (16), may be articulated in the following manner:

$$\begin{cases} \dfrac{di_d}{dt} = \dfrac{1}{L_d}\left(v_d - R_s i_d + P w_r L_q i_q\right) - \dfrac{1}{L_d} F_d, \\ \dfrac{di_q}{dt} = \dfrac{1}{L_q}\left(v_q - R_s i_q - P w_r L_d i_d - P w_r \phi_f\right) - \dfrac{1}{L_q} F_q. \end{cases} \tag{17}$$

The components F_d and F_q correspond to fluctuations in parameters and are expounded as follows:

$$\begin{cases} F_d = \Delta L_d \dfrac{di_d}{dt} - \Delta L_q P w_r i_q + \Delta R_s i_d, \\ F_q = \Delta L_q \dfrac{di_q}{dt} + \Delta L_d P w_r i_d + \Delta R_s i_q + \Delta \phi_f P w_r. \end{cases} \tag{18}$$

In the absence of a precise understanding of the dynamics underlying various uncertainties, it is postulated that their progression occurs at a comparatively gradual pace in relation to the system's time constants. Consequently, we may express it as follows:

$$\begin{cases} \dfrac{dF_d}{dt} = 0, \\ \dfrac{dF_q}{dt} = 0. \end{cases} \tag{19}$$

The bilinear system that represents the electrical subsystem could be written in the following form:

$$\left\{ \dot{x}(t) = f(x, \omega_r) + g_1 u(t) + g_2 F(t),\ y_i(t) = h_i(x), i = 1,2, \right. \tag{20}$$

with: $x(t) = \begin{bmatrix} i_d \\ i_q \end{bmatrix}$ is the vector of states; $y(t) = \begin{bmatrix} y_1(t) \\ y_2(t) \end{bmatrix} = \begin{bmatrix} h_1(x) \\ h_2(x) \end{bmatrix} = \begin{bmatrix} i_d \\ i_q \end{bmatrix}$ is the output vector; the controlling vector is $u(t) = \begin{bmatrix} V_d \\ V_q \end{bmatrix}$; $g_1 = [g_d g_q] = \begin{bmatrix} 1/L_d & 0 \\ 0 & 1/L_q \end{bmatrix}$, g_2

$= \begin{bmatrix} -1/L_d & 0 \\ 0 & -1/L_q \end{bmatrix}$; the vector field f is given by $f(x, \omega_r) = \begin{bmatrix} f_1(x) \\ f_2(x) \end{bmatrix} = \begin{bmatrix} -R_S/L_d i_d + L_q/L_d p\omega_r i_q \\ -R_S/L_q i_q - L_d/L_q p\omega_r i_d - \varphi_f p\omega_r/L_q \end{bmatrix}$; the vector of disturbances caused by the parameter variations is $F(t) = \begin{bmatrix} F_d \\ F_q \end{bmatrix}$. The objective of the controller is the regulation of the current components, which means that the output vector is $y(t) = \begin{bmatrix} y_1(t) \\ y_2(t) \end{bmatrix} = \begin{bmatrix} h_1(x) \\ h_2(x) \end{bmatrix} = \begin{bmatrix} i_d(t) \\ i_q(t) \end{bmatrix}$.

To surmount the challenge of real-time computation and attain a closed-form optimal nonlinear generalized predictive control (NGPC), a novel approach has been posited. This method involves the constraint of control order to zero, thereby ensuring the constancy of control effort within the prediction interval. An analytical solution can be derived by setting the prediction horizon to zero. Predictive control's fundamental objective lies in the computation of control $u(t)$ such that the forthcoming motor outputs, denoted as $y(t+\tau)$ for $0 \le \tau \le T_r$, converge towards $y_r(t+\tau)$, all while taking into account the presence of perturbations. This objective is realized through the minimization of the cost function $\mathfrak{J}$ over a prediction horizon of time T_r [37].

$$\mathfrak{J}(x,u) = \frac{1}{2}\int_0^{T_r} \left(y_r(t+\tau) - y(t+\tau)\right)^T \left(y_r(t+\tau) - y(t+\tau)\right) d\tau, \tag{21}$$

with: $y_r(t) = \begin{bmatrix} y_{1r}(t) \\ y_{2r}(t) \end{bmatrix} = \begin{bmatrix} i_{dr} \\ i_{qr} \end{bmatrix}$, $y(t) = \begin{bmatrix} y_1(t) \\ y_2(t) \end{bmatrix} = \begin{bmatrix} h_1(t) \\ h_2(t) \end{bmatrix} = \begin{bmatrix} i_d \\ i_q \end{bmatrix}$, and T_r signifies the prediction time horizon, wherein $y_r(t+\tau)$ signifies the envisioned future reference trajectory, while $y(t+\tau)$ signifies the anticipated value of the system's output τ steps ahead. Consequently, the quadratic performance index embodied in the cost function $\mathfrak{J}$ undergoes a modification as follows:

$$\mathfrak{J}(x,u) = \frac{1}{2}\int_0^{T_{r1}} \left(y_{1r}(t+\tau) - y_1(t+\tau)\right)^2 d\tau + \frac{1}{2}\int_0^{T_{r2}} \left(y_{2r}(t+\tau) - y_2(t+\tau)\right)^2 d\tau. \tag{22}$$

The prediction of the output is computed through the utilization of a Taylor series expansion:

$$y_i(t+\tau) = h_i(x) + \tau L_f h_i(x) + \frac{\tau^2}{2!}L_f^2 h_i(x) + \ldots + \frac{\tau^{\rho_i}}{\rho_i!}L_f^{\rho_i} h_i(x) + \frac{\tau^{\rho_i}}{\rho_i!}L_g L_f^{\rho_i - 1} h_i(x) u(t). \tag{23}$$

Let us denote ρ_i the relative degree of each output $y_i(t)$: $i = 1, 2$, which determines the number of times the output must be differentiated before the input u appears. The Lie derivative of the functions $h_k(x)$ along a vector field is denoted using the following notation: $f(x) = (f_1(x) \ldots f_n(x))$ [32].

We allow ρ_i to represent the relative degree associated with each output $y_i(t)$: $i = 1, 2$, a parameter that signifies the number of differentiations the output $y\_i(t)$ must undergo prior to the input u becoming apparent:

$$\begin{cases} L_f h_k(x) = \sum_{i=1}^{n} \dfrac{\partial h_k(x)}{\partial x_i} f_i(x), L_f^k h_k(x) = L_f\left(L_f^{k-1} h_k(x)\right), L_g L_f h_k(x) = \dfrac{\partial L_f h_k(x)}{\partial x} g(x). \end{cases} \tag{24}$$

Employing equation (20):

$$\begin{cases} \dot{y}_1\ (t) = L_f h_1(x) + L_{g_1} h_1(x) u(t) + L_{g_2} h_1(x) F(t), \\ \dot{y}_2\ (t) = L_f h_2(x) + L_{g_1} h_2(x) u(t) + L_{g_2} h_2(x) F(t). \end{cases} \tag{25}$$

The relative degree of the outputs $y_1(t)$ and $y_2(t)$ is denoted as $\rho_{1,2} = 1$. This signifies that the Lie derivatives of the functions $h_k(x)$ are nonzero and may be articulated as follows:

$$y_1(t+\tau) = h_1(x) + \tau\left[L_f h_1(x) + L_{g_1} h_1(x) u(t) + L_{g_2} h_1(x) F(t)\right], \tag{26}$$

$$y_2(t+\tau) = h_2(x) + \tau\left[L_f h_2(x) + L_{g_1} h_2(x) u(t) + L_{g_2} h_2(x) F(t)\right]. \tag{27}$$

In order to ascertain the optimal order, it is imperative to satisfy the following prerequisite conditions:

$$\frac{\partial \Im(x,u)}{\partial u} = 0. \tag{28}$$

By integrating equations (26) and (27) into equation (22) and subsequently minimizing the cost function (22), the resultant optimal nonlinear control can be elucidated as follows:

$$u(t) = H_1(x)^{-1}\left[\sum_{i=0}^{1} Z_i^1\left(y_{1r}^{(i)}(t) - L_f^{(i)} h_1(x)\right) - K_1 F(t) \sum_{i=0}^{1} Z_i^2\left(y_{2r}^{(i)}(t) - L_f^{(i)} h_2(x)\right) - K_2 F(t)\right]. \tag{29}$$

With:

$$\begin{cases} Z_0^1 = \dfrac{3}{2T_{r1}}; Z_1^1 = 1, \\ \\ Z_0^2 = \dfrac{3}{2T_{r2}}; Z_1^2 = 1. \end{cases} \tag{30}$$

The matrixes K_1, K_2, and $H_1(x)$ are presented as follows:

$$\begin{aligned} K_1 &= L_{g_2} h_1(x) = \begin{bmatrix} \dfrac{-1}{L_d} & 0 \end{bmatrix}, \\ K_2 &= L_{g_2} h_2(x) = \begin{bmatrix} 0 & \dfrac{-1}{L_q} \end{bmatrix}, \\ H_1(x) &= \begin{bmatrix} L_{g_1} h_1(x) \\ L_{g_1} h_2(x) \end{bmatrix} = \begin{bmatrix} \dfrac{1}{L_d} & 0 \\ 0 & \dfrac{1}{L_q} \end{bmatrix}. \end{aligned} \tag{31}$$

The poles of the characteristic equation are as follows: $s_d = -3/2T_{r1}$; $s_q = -3/2T_{r2}$. The closed-loop system attains asymptotic stability owing to the presence of negative real parts in all of its poles. When knowledge of the disturbance is available, the dynamics of the tracking error are solely dictated by the prediction time, with a quicker response corresponding to a shorter prediction time. Nevertheless, even when the resistive torque is known, the identification of uncertainties and model variations remains a challenging task, necessitating the intervention of an observer. The incorporation of disturbance compensation in the controller is intricate due to the relative degree of the disturbance being lower than that of the input [32]. Furthermore, if the disturbance is neglected within the controller, it leads to a steady-state error in the closed-loop system, as delineated in the ensuing equation:

$$\begin{cases} \lim\limits_{t \longrightarrow \infty^+} e_1(t) = \lim\limits_{t \longrightarrow \infty^+} \dfrac{-K_1 F(t)}{Z_0^1}, \\ \\ \lim\limits_{t \longrightarrow \infty^+} e_2(t) = \lim\limits_{t \longrightarrow \infty^+} \dfrac{-K_2 F(t)}{Z_0^2}. \end{cases} \tag{33}$$

3.4. Stability Analysis. To analyze the stability of the closed-loop system, it is necessary to determine the tracking errors at the origin. This can be achieved by obtaining the characteristic equation of the closed-loop system, which is derived by substituting equation (29) into equation (25):

$$\begin{cases} Z_1^1 s + Z_0^1 = 0, \\ Z_1^2 s + Z_0^2 = 0. \end{cases} \tag{32}$$

3.5. Robust Nonlinear Generalized Predictive Control Design (RNGPC). The principal limitation of the aforementioned classical predictive control resides in its reliance upon acquiring knowledge about disturbances, a task that proves challenging to procure and must be estimated through the expertise of an observer. This challenge escalates in situations where the perturbation rate lags behind that of the primary source, as exemplified in the context of PMSM. In such instances, crafting a precise disturbance observation

becomes an undertaking, leading to a heightened level of complexity in the design of the closed-loop system.

To improve disturbance mitigation, we have introduced an integral action within the controller. The noteworthy attribute of this proposed control scheme is its capability to enhance robustness without the need for explicit knowledge of external disturbances and parameter uncertainties. The research methodology employed comprises five principal steps, as depicted in Figure 2.

The quadrature criterion translating the objective of the internal loop that is proposed is written in the following form:

$$J(x,u) = \frac{1}{2}\int_0^{T_{r1}} I_d(t+\tau)^2 d\tau + \frac{1}{2}\int_0^{T_{r2}} I_q(t+\tau)^2 d\tau, \quad (34)$$

where T_{r1}, T_{r2} are the prediction time for output 1 and 2, respectively. The integral of the sortie error is $I_i(t) = \int_0^t e_i(\tau)d\tau\, i = d,\ q$. The sortie error with y_{ri} the desired trajectory and y_i the system output is $e_i(\tau) = (y_{ri}(\tau) - y_i(\tau))i = d,\ q$, with $y(t+\tau), y_r(t+\tau)$ are the prediction at τ steps ahead of the system output and that of the desired trajectory in the future, respectively.

The predicted value of $I_i(t+\tau)$ in this case is obtained by a Taylor series expansion with $(\rho_i + 1)$.

$$I_i(t+\tau) = \sum_{j=0}^{\rho_i+1} \frac{\tau^j}{j!} I_i^{(j)}(t). \quad (35)$$

If we disregard the disturbance, the expression (25) leads to the following equation:

$$\begin{cases} \dot{y}_1(t) = L_f h_1(x) + L_{g_1} h_1(x) u(t), \\ \dot{y}_2(t) = L_f h_2(x) + L_{g_1} h_2(x) u(t). \end{cases} \quad (36)$$

The predicted $I_i(t+\tau)$ term is calculated by the following equation:

$$I(t+\tau) = \begin{bmatrix} I_d(t+\tau) \\ I_q(t+\tau) \end{bmatrix} = \mathrm{T}(\tau) Y(t), \quad (37)$$

with:

$$\mathrm{T}(\tau) = \begin{bmatrix} 1 & 0 & \tau & 0 & \frac{\tau^2}{2!} & 0 \\ 0 & 1 & 0 & \tau & 0 & \frac{\tau^2}{2!} \end{bmatrix} = \begin{bmatrix} \urcorner_1(\tau) \\ \urcorner_2(\tau) \end{bmatrix},$$

$$Y(t) = \begin{bmatrix} \int_0^t e_1(\tau)d\tau & \int_0^t e_2(\tau)d\tau & e_1(t) & e_2(t) & e_1^{\cdot}(t) & e_2^{\cdot}(t) \end{bmatrix}^T. \quad (38)$$

Using the equation (37) in the cost function (34), we will have the following equation:

$$J(x,u) = \frac{1}{2}\left[Y(t)^T \nabla(T_{r1}, T_{r2}) Y(t)\right], \quad (39)$$

with:

$$\nabla(T_{r1}, T_{r2}) = \int_0^{T_{r1}} \urcorner_1(\tau)^T \urcorner_1(\tau) d\tau + \int_0^{T_{r2}} \urcorner_2(\tau)^T \urcorner_2(\tau) d\tau. \quad (40)$$

In order to find the optimal order, we must satisfy the following necessary conditions:

$$\frac{\partial J(x,u)}{\partial u} = 0. \quad (41)$$

By directly applying the control law defined by (39), we obtain the following optimal control law in the sense of the criterion (41):

$$u(t) = \left(L_{g_1} h(x)\right)^{-1} \left[Z_0^1 \int_0^t e_d(\tau)d\tau + \sum_{i=1}^{2} Z_i^1 \left({y_{dr}}^{(i-1)}(t) - {L_f}^{(i-1)} h_1(x) \right) Z_0^2 \int_0^t e_q(\tau)d\tau + \sum_{i=1}^{2} Z_i^2 \left({y_{qr}}^{(i-1)}(t) - {L_f}^{(i-1)} h_2(x) \right) \right], \quad (42)$$

with:

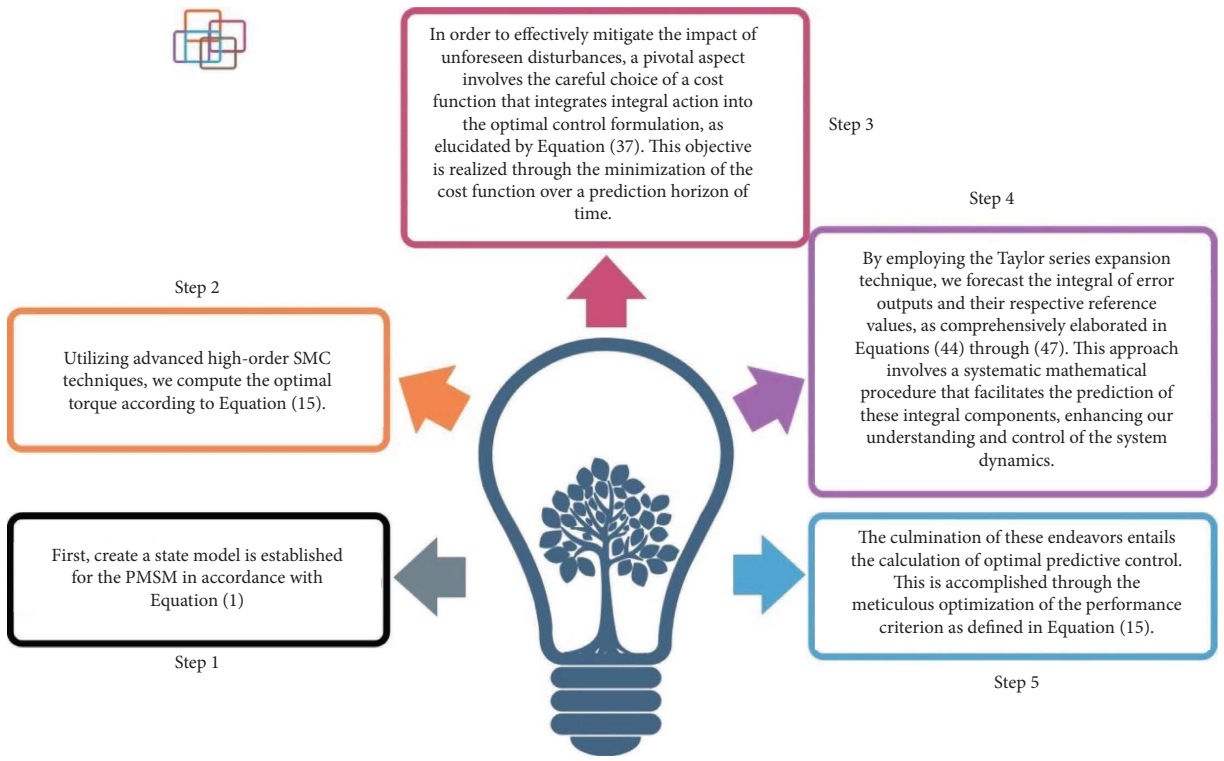

Figure 2: Control design methodology.

$$\begin{cases} Z_0^1 = \dfrac{10}{3T_{r1}^2};\ Z_1^1 = \dfrac{5}{2T_{r1}};\ Z_2^1 = 1, \\ Z_0^2 = \dfrac{10}{3T_{r2}^2};\ Z_1^2 = \dfrac{5}{2T_{r2}};\ Z_2^2 = 1, \\ L_{g_1}h(x) = \begin{bmatrix} L_{g_1}h_1(x) \\ L_{g_1}h_2(x) \end{bmatrix} = \begin{bmatrix} \dfrac{1}{L_d} & 0 \\ 0 & \dfrac{1}{L_q} \end{bmatrix}, \\ L_{\mathbf{f}}h_1(x) = \dfrac{-R_S}{L_d}i_d + \dfrac{L_q}{L_d}p\omega_r i_q, \\ L_{\mathbf{f}}h_2(x) = \dfrac{-R_S}{L_q}i_q - \dfrac{L_d}{L_q}p\omega_r i_d - \dfrac{\boldsymbol{\varphi}_{\mathbf{f}}p\omega_r}{L_q}. \end{cases} \tag{43}$$

The control design methodology encompasses several key steps as shown in Figure 2. First, a state model is established for the PMSM in accordance with equation (1). Next, leveraging high-order sliding mode control, the optimal torque is calculated as outlined in equation (14). To address the influence of unknown disturbances, a crucial step involves the selection of a suitable cost function that incorporates integral action within the optimal control expression, as described by equation (34). Employing Taylor series development, the integral of error outputs and their corresponding references are predicted, as detailed in equations (39)–(42). The culmination of these efforts involves the computation of optimal predictive control, achieved by optimizing the performance criterion articulated in equation (14).

The proposed new controller incorporates integral action; therefore, if the closed-loop system is stable, the steady-state error is eliminated despite the unknown disturbances. Therefore, it is simple to construct the controller provided by (42) since no disturbances are included.

3.6. The Closed-Loop System's Stability. To assess the stability of the closed-loop system, it is necessary to look at the stability of the output tracking errors at the origin. The following characteristic equation of the closed-loop system of the outer loop is produced by substituting (42) into (36):

$$\begin{cases} Z_2^1 s^2 + Z_1^1 s + Z_0^1 = 0, \\ Z_2^2 s^2 + Z_1^2 s + Z_0^2 = 0. \end{cases} \tag{44}$$

The poles of the characteristic equation are as follows:

$$\begin{aligned} s_d &= \frac{-1.25 \mp 1.3307i}{Tr_1}; \\ s_q &= \frac{-1.25 \mp 1.3307i}{Tr_2}. \end{aligned} \tag{45}$$

Because every poll has a negative real portion, the closed-loop system is asymptotically stable. In the case where the disturbance is known, the dynamics of the tracking error depend only on prediction time. The smaller the prediction time, the faster the response.

4. Simulation results

Simulations were run using the Matlab/Simulink program to assess the effectiveness and performance of the suggested control. The predictive times T_{r1} and T_{r2} are taken 0.7 ms. The sampling time of the controller T_C and the sampling time in the mathematical model of the PMSM T_S are chosen equal to 10^{-5}s. The pole placement approach is used to determine the HSMC gains a_1 and a_2. The values used are $a_1 = 13$ and $a_2 = 2000$. The reference trajectory tracking performances are studied under unknown load torque and parameter uncertainties. The reference velocity passes through a filter so that the dynamics of the reference trajectory are adequate, and this avoids a strong phase current. The motor is driven by a voltage inverter under PWM control, and the parameters of the investigated PMSM are specified in Table 1.

Table 1: System parameters.

PMSM parameter	Value
Nominal power (P_n)	250 w
Rated current (I_n)	5.7 A
Rated voltage (V_n)	42 V
Rated speed (N)	4000 rad/min
Stator inductance (L_d)	0.00025 H
Stator inductance (L_q)	0.00025 H
Pole pairs number (p)	5
Flux linkage (φ_f)	0.015921 Wb
Total inertia (J)	2.9127×10^{-4} kg.m^2
Stator resistance (R_s)	0.1811 Ω
Coefficient of friction (f)	3.6345×10^{-4} N.m.s/rad

4.1. Performance Evaluation for Constants Parameter Values. Within the dedicated section, we engage in a comprehensive assessment of the proposed controller's performance while the PMSM operates with fixed parameters under varying load torque conditions. This rigorous evaluation is a critical component of our research, aiming to provide a deep understanding of how the controller responds to different load scenarios.

Throughout this section, we meticulously investigate the system's behavior across specific time intervals, each representing a distinct phase of our analysis. These time intervals are denoted as tϵ [0 1] s, [1 3] s, [3 6] s, [7 9] s, and [9 12] s, and they play a pivotal role in our evaluation framework. Within each interval, we precisely define the magnitude of the resistive torque applied to the PMSM. The resistive torque profiles are as follows:

(i) In the initial time interval [0 1] s, the system operates under a constant resistive torque of 0 Nm

(ii) Moving to the interval [1 3] s, the resistive torque is elevated to 0.5 Nm

(iii) During the subsequent phase of [3 6] s, the resistive torque returns to 0 Nm

(iv) As we progress to [7 9] s, the system experiences another episode of resistive torque, set at 0.5 Nm

(v) Finally, in the concluding interval of [9 12] s, the resistive torque is once again reduced to 0 Nm

This meticulous approach to performance evaluation enables us to gain in-depth insights into how the proposed controller reacts to varying load torque conditions. It empowers us to draw meaningful conclusions regarding the controller's effectiveness, stability, and adaptability across a spectrum of real-world operational scenarios. These findings contribute significantly to the broader understanding of our research outcomes and the controller's potential applications.

Figure 3 showcases the simulation outcomes for the velocity trajectory tracking of RNGPC and the proposed control while accounting for varying load torque. Notably, the proposed controller effectively neutralizes the influence exerted by the resistive torque. Remarkably, the speed signal demonstrates an impressively prompt response time, seamlessly maintaining its reference point with an exceptionally brief latency.

Figure 4 shows the simulation outcomes for the speed trajectory tracking error, measured in (pu), of both RNGPC and the proposed control, while accounting for varying load torque. As depicted in the graphs, in both control strategies, the error swiftly converges to 0 within a remarkably short timeframe and attains a steady state of zero for every change in load torque. However, it is worth noting that the proposed control exhibits superior error convergence to 0 compared to RNGPC across all variations in load torque. Figure 5 shows the simulation outcomes for the electromagnetic torque and load torque, comparing the performance of RNGPC and the proposed control under varying resistive torque conditions. From the depicted plots, it is evident that the electromagnetic torque progressively rises until it reaches a magnitude equivalent to the combined load torque and friction, thereby precisely tracking their values.

Figure 6 illustrates the simulation outcomes for the stator current components, i_q and i_d, under the influence of varying load torque, specifically with the implementation of the proposed control. The figure highlights that, with the proposed control, the i_d component remains consistently aligned with its reference value of zero across all load torque variations. Additionally, the i_q component aligns itself with its reference value, denoted as i_{qref}, and impeccably tracks it for every change in load torque. It is worth noting that the oscillations observed in the signals are attributed to the motor supply inverter, while the peaks are a consequence of the form of the setpoint speed. Notably, the proposed method delivers commendable performance, ensuring stability across all signals.

Figure 7 exhibits the simulation outcomes depicting the evolution of the current i_a for both RNGPC and the proposed control, considering variations in load torque. Notably, the proposed control demonstrates commendable performance, ensuring stability across all signals. Consequently, the observed peaks can be attributed to the specific shape or form of the input.

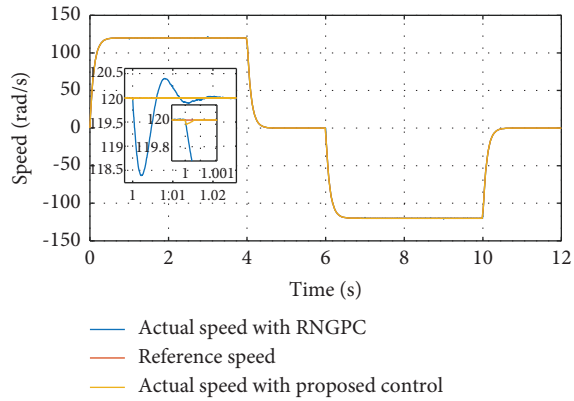

Figure 3: Speed tracking.

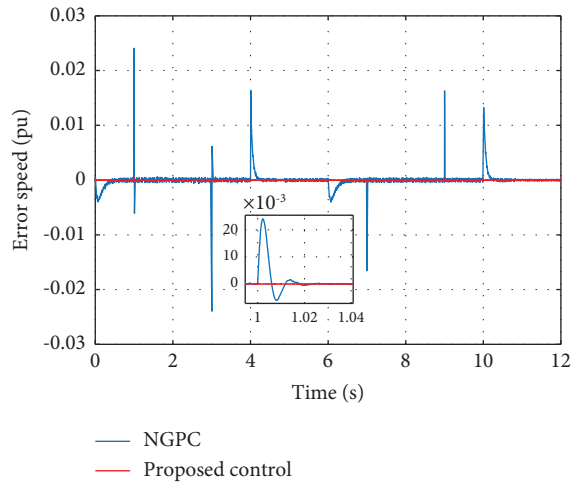

Figure 4: The error in velocity.

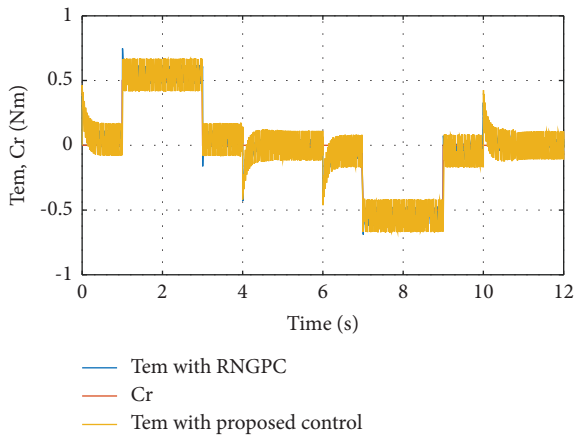

Figure 5: The progression of the resistive torque (Cr) and the electromagnetic torque (Tem).

4.2. Robustness Tests. To comprehensively examine the mathematical model of the PMSM, a series of simulations were conducted, encompassing various parameter variations. In each simulation, a single parameter was modified within the time interval $t \epsilon$ [5 7] s. Specifically, the robustness tests involved altering the stator resistance Rs by +100%, decreasing the magnet flux by −20%, and increasing the coefficient of viscous friction f by +5%. Furthermore, the load torque was set to 1 Nm within the time range of $t \epsilon$ [2 7] s, while a setpoint step of 120 rads/s was applied for each test.

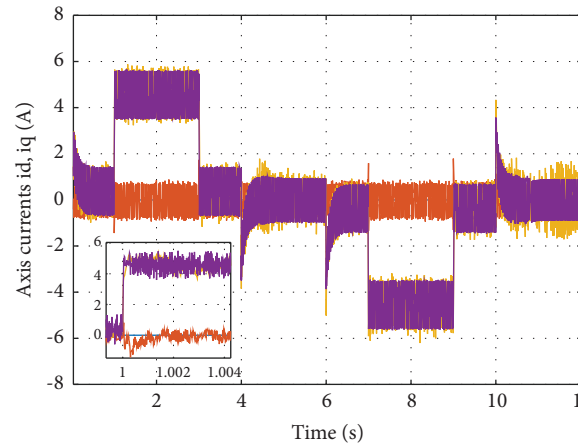

Figure 6: The axis components of i_d and i_q.

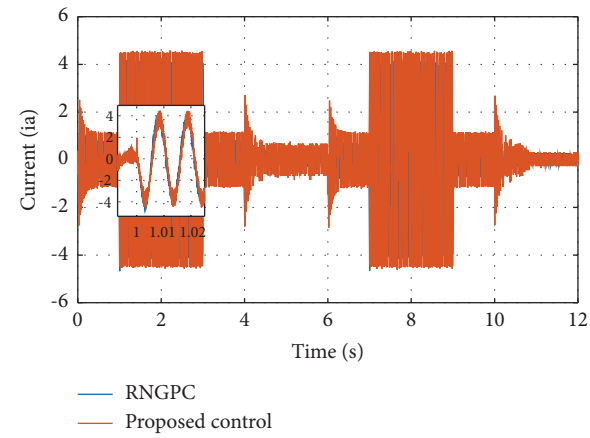

Figure 7: The evolution of the armature current (i_a).

Figure 8 presents the simulation results for the velocity trajectory tracking of both RNGPC and the proposed control, considering fluctuations in both load torque and machine parameters. The visual representations within Figure 8 lead to the conclusion that the motor speed adeptly tracks its desired trajectory, demonstrating a rapid response and effective rejection of disturbances for both control algorithms. Nonetheless, it is evident that the proposed algorithm exhibits enhanced stability attributes, characterized by a robust response and proficient disturbance rejection capabilities.

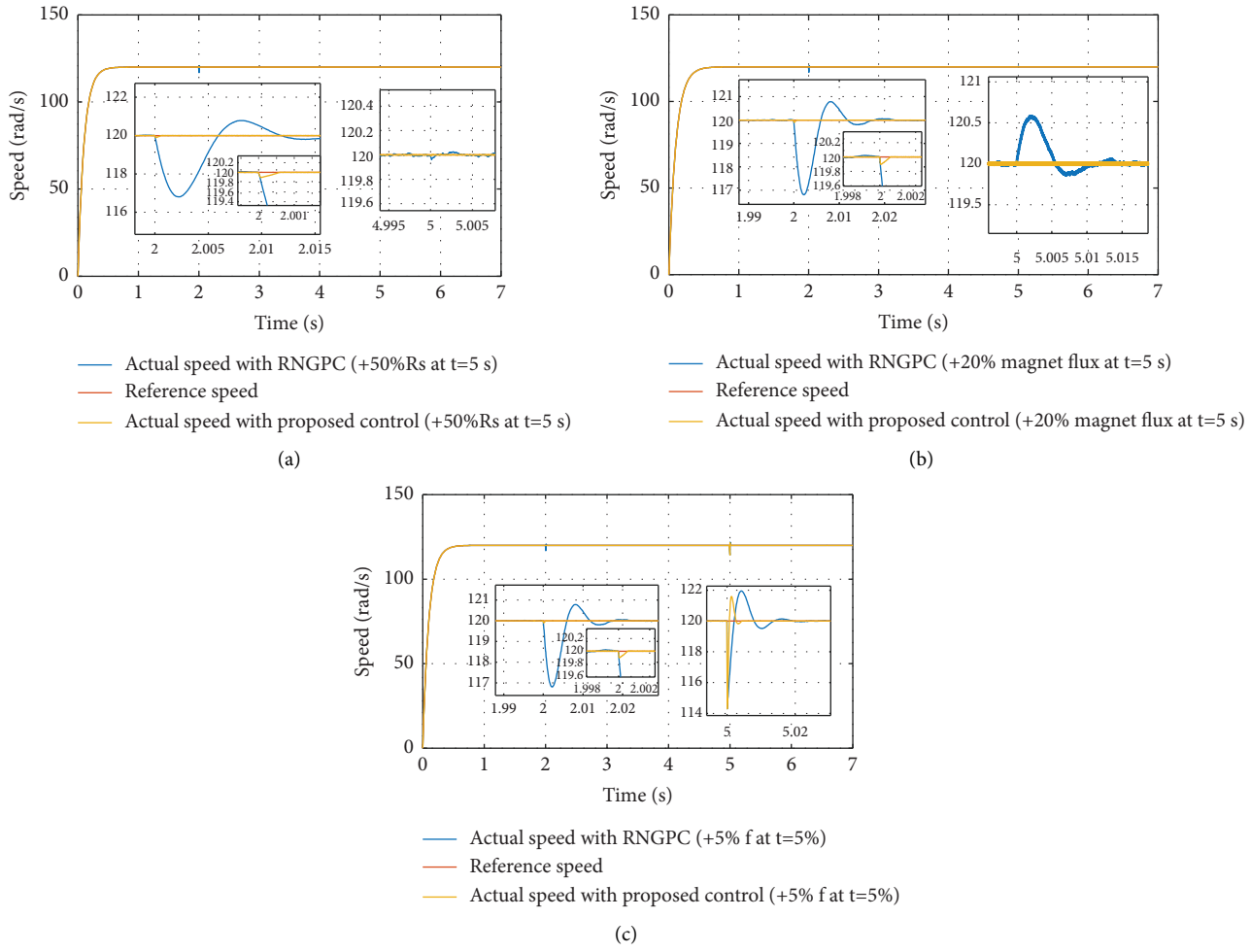

Figure 8: The speed of lead torque 1 Nm at $t \epsilon$ [2 7] s and at $t \epsilon$ [5 7] s. (a) +50% of Rs, (b) +20% of the flux, and (c) +5% of the coefficient of the viscous friction.

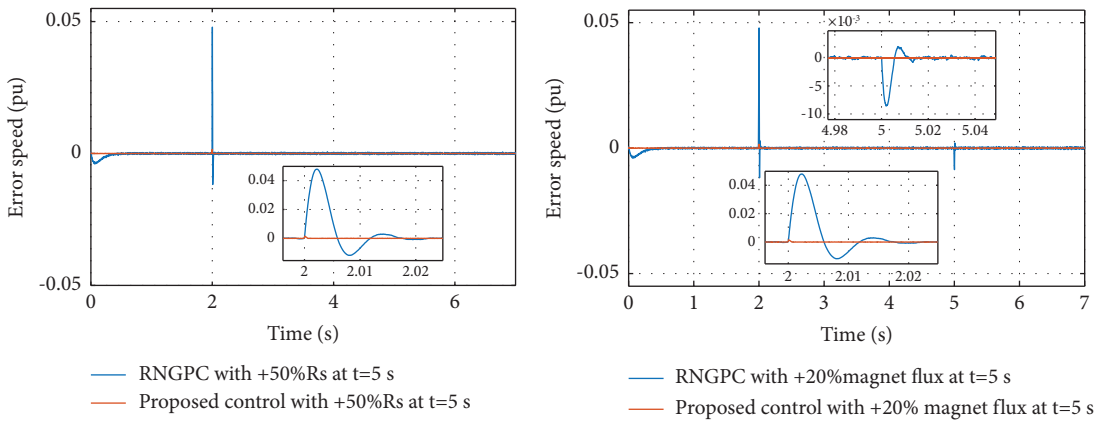

Figure 9: Continued.

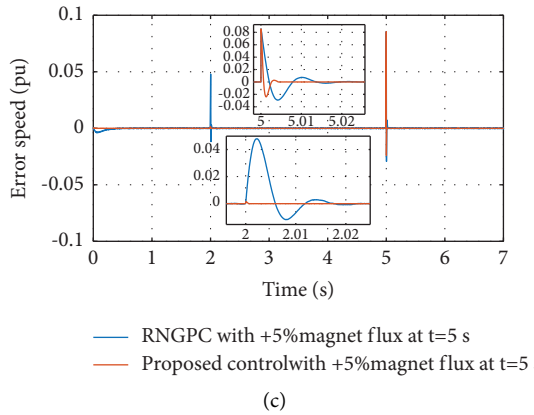

FIGURE 9: The evolution of the speed error with the RNGPC and the proposed control. (a) +50% of Rs, (b) +20% of the flux, and (c) +5% of the coefficient of the viscous friction.

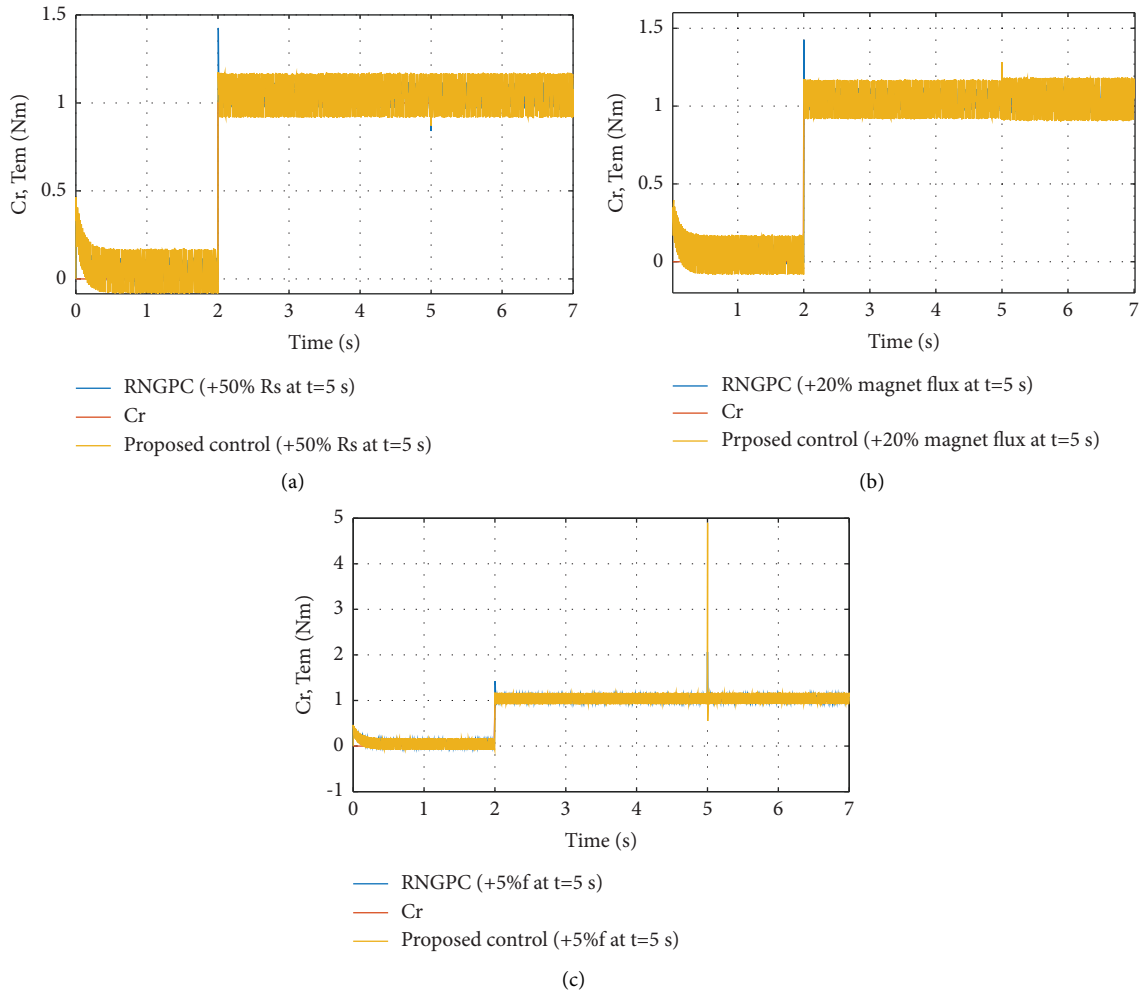

FIGURE 10: The evolution of Cr and Tem with RNGPC and the proposed control. (a) +50% of Rs, (b) +20% of the flux, and (c) +5% of the coefficient of the viscous friction.

Figure 9 depicts the simulation results for the speed trajectory tracking error, measured in (pu), comparing the performance of RNGPC and the proposed control across variations in resistive torque and machine parameters. The results clearly indicate that the proposed control exhibits significantly lower speed tracking errors compared to

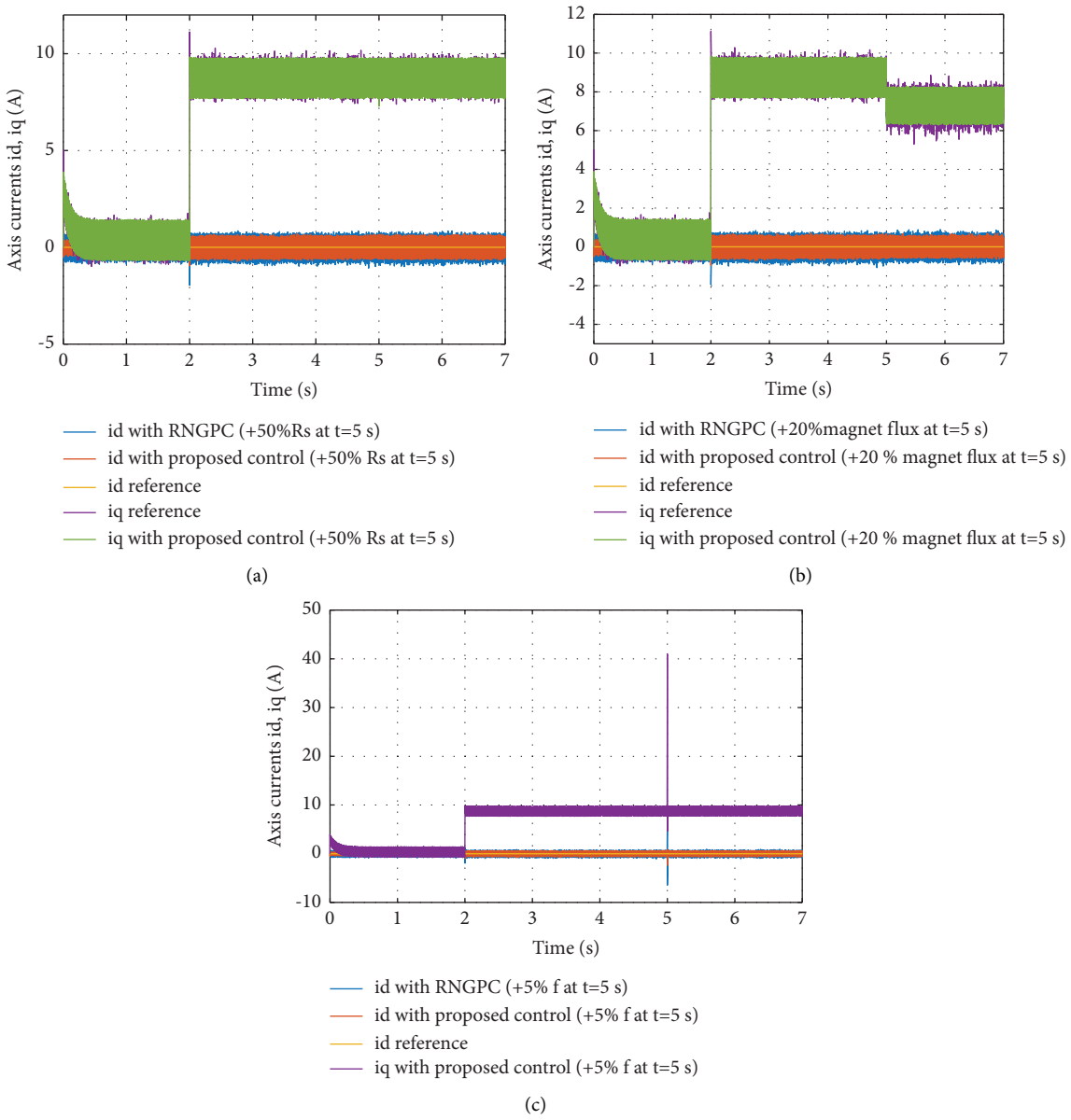

Figure 11: The components of the i_d and i_q axes. (a) +50% of Rs, (b) +20% of the flux, and (c) +5% of the coefficient of the viscous friction.

RNGPC. Furthermore, the error converges rapidly to zero and eventually achieves a steady state. Figure 10 presents the simulation results for the electromagnetic torque and load torque of the machine under the influence of variations in resistive torque and machine parameters. Both the proposed control and RNGPC are displayed in the graphs. As observed, the electromagnetic torque gradually increases until it reaches a magnitude equivalent to the combined load torque and friction, precisely aligning with these values.

Figure 11 shows the armature current components, i_d and i_q axis, for different variations in resistive torque and machine parameters, as observed in both RNGPC and the proposed control. Upon careful examination, it is evident that the i_d axis component remains consistently at zero for all variations in load torque and machine parameters. However, it is noteworthy that the i_q axis component fails to accurately track its reference value under these conditions. To assess the quality of the controlled responses, two commonly used metrics, namely, the integral time-weighted absolute error (ITAE) and integral squared error (ISE), were employed in conjunction with different control strategies. The corresponding results are presented in Figures 12 and 13. These findings clearly demonstrate that the responses obtained through the proposed strategy generally outperform those obtained by other techniques, including NGPC with observer and RNGPC.

The findings presented in this study support the objectives outlined in the introduction section, confirming the efficacy of the proposed technique. Specifically, the suggested approach successfully achieves the goals of maintaining the motor speed at its designated reference value and ensuring the efficient, secure, and reliable operation of the

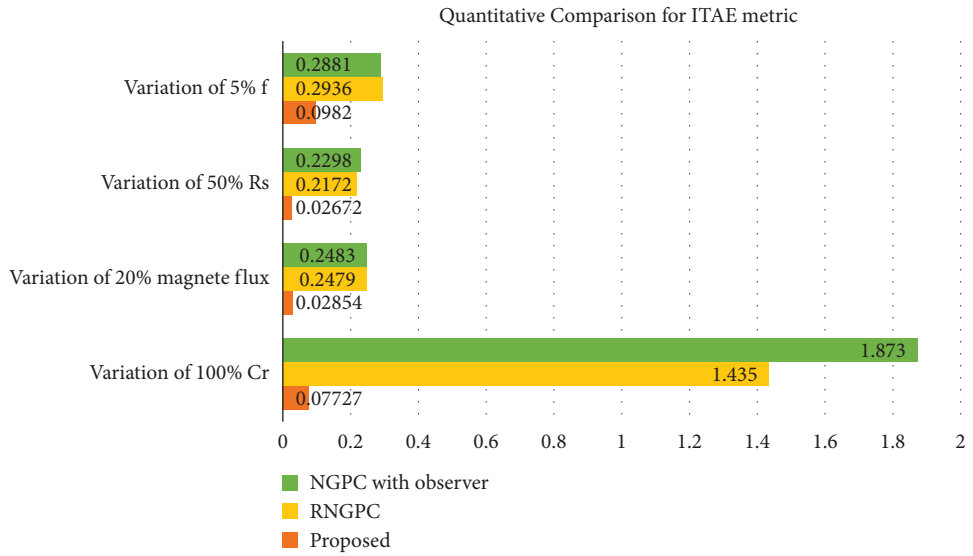

Figure 12: The quantitative comparison for the ITAE metric. ITAE, integral time-weighted absolute error.

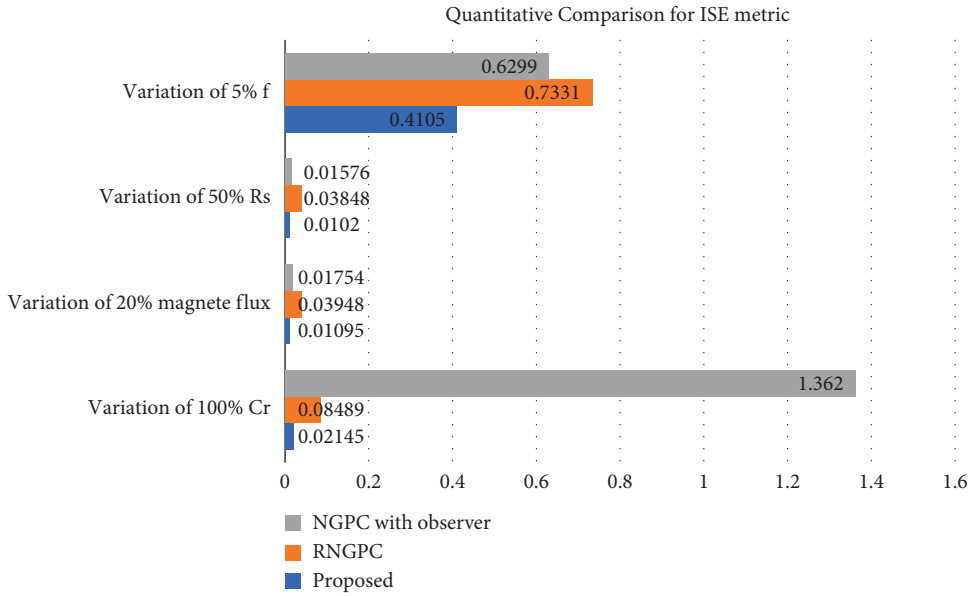

Figure 13: The quantitative comparison for ISE metric. ISE, integral squared error.

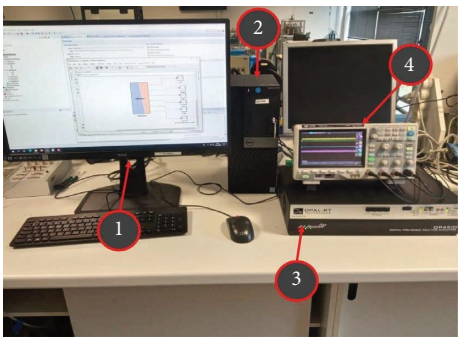

Figure 14: Real-time testing results using OPAL-RT.

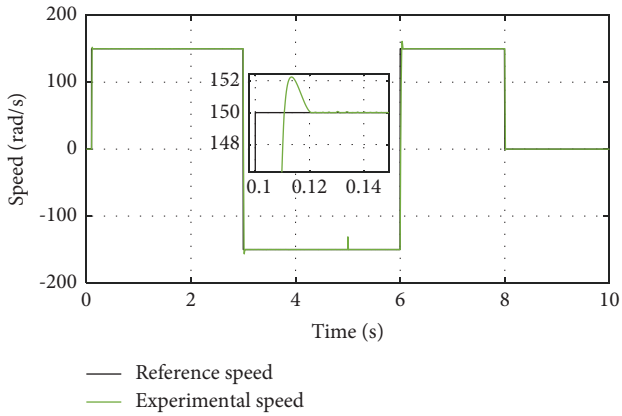

Figure 15: Real-time testing of PMSM speed.

PMSM, even in the presence of potential electrical power disruptions.

5. Experimental Results

The OPAL-RT system employs hardware-in-the-loop (HIL) simulation, bridging software-based simulations and real-world hardware. It integrates the OP 4510 board and related components into a real-time simulation environment. This board incorporates powerful field-programmable gate array (FPGA) blocks for emulating and interacting with simulated systems. The RT-Lab interface links MATLAB/Simulink to real-time hardware, enabling interactive feedback between virtual models and physical components. HIL simulation with OPAL-RT is valuable for testing control algorithms, validating designs, analyzing complex systems, and reducing the need for costly real-world testing [41, 42].

The configuration of the real-time simulator setup is depicted in Figure 14. It involves several integral components, namely, (1) the MATLAB/Simulink software and RT-Lab platform for execution, (2) a host PC, (3) the OPAL-RT 4510 equipment, and (4) a digital oscilloscope. The process unfolded with the decomposition and adaptation of the PMSM simulation system for integration into the RT-Lab platform, eventually culminating in the execution of real-time simulations.

The experimental framework was further manifested through Figures 15–17, which show the results obtained from the proposed technique when subjected to perturbations in load torque. Remarkably, the outcomes derived from the discrete real-time simulator, RT-LAB, exhibit a remarkable proximity to the results anticipated from the simulation. This underscores the fidelity and accuracy of the real-time simulation process facilitated by the OPAL-RT system.

Figure 15 shows the simulation results pertaining to rotor speed trajectory tracking. The plot clearly demonstrates the remarkable fidelity between the actual rotor speed and the reference trajectory. Even in the presence of load torque, the control system effectively eliminates steady-state errors, ensuring precise tracking. Moving to Figure 16, we delve into the evolution of electromagnetic torque. Here, the measured torque exhibits an impressive performance by closely tracking its reference with minimal ripple, even when dealing with abrupt trajectory changes. This observation underscores the robustness and accuracy of the control approach in maintaining torque control objectives. The simulation results for the d-axis component of the armature current are presented in Figure 17. Notably, the d-axis current component remains consistently aligned with its prescribed reference, demonstrating the controller's ability to maintain desired current values accurately.

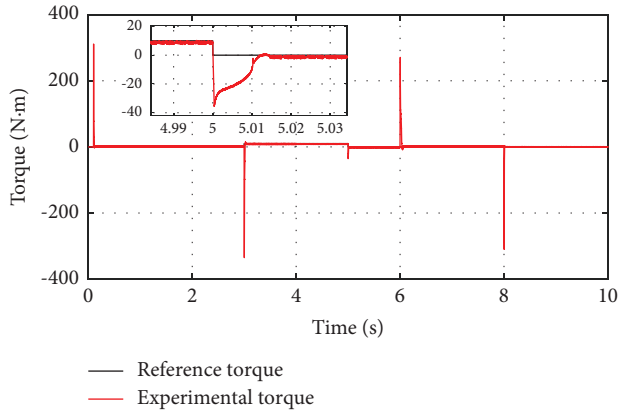

Figure 16: Real-time response of PMSM torque.

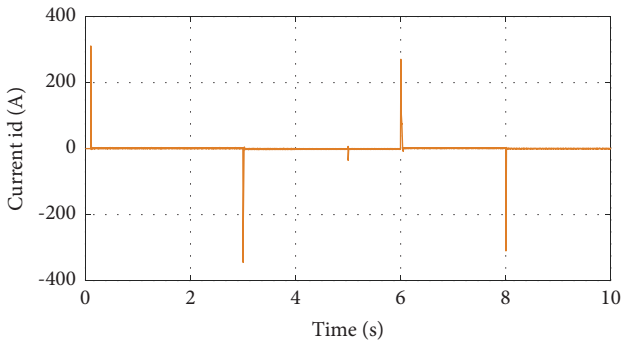

Figure 17: Real-time response of the direct current.

Thus, these experimental findings serve as compelling evidence of the validity and effectiveness of the proposed control approach. The close agreement between simulation and experimental results attests to the robustness and real-time applicability of the control strategy, reaffirming its potential for practical implementation in various motor control applications.

6. Conclusion

This paper introduces an innovative control approach that combines HSMC with generalized nonlinear robust predictive control (RNGPC) for the PMSM. The primary control objective is to achieve accurate speed tracking and ensure robustness against external disturbances and parameter uncertainties. To accomplish this, the HSMC controller is first employed to determine the current reference (i_{qref}), followed by the utilization of the RNGPC controller to determine the reference voltage. A key contribution of this work is the introduction of a novel finite horizon cost function for RNGPC, which incorporates integral action in the control loop, thereby enhancing robustness against parametric uncertainties and external disturbances.

One notable feature of this method is its independence from a disturbance observer, yet it significantly enhances disturbance rejection and robustness against parameter variations. This unique aspect of the proposed approach sets it apart in the realm of motor control strategies. To thoroughly assess the effectiveness of the proposed controller, comprehensive testing is conducted under diverse operating conditions, including scenarios with mismatched parameters and external disturbances. To provide a clearer analysis and discussion of the presented results, we introduce performance indices and metrics that highlight the controller's capabilities:

(i) Tracking Performance: The tracking error, represented as the deviation between the actual speed and the reference trajectory, is a critical metric. The results demonstrate that the proposed control approach exhibits minimal tracking errors, signifying its ability to accurately track desired speed profiles.

(ii) Robustness Evaluation**: Robustness is evaluated by introducing external disturbances and parameter uncertainties. Metrics such as disturbance rejection ratios and parameter sensitivity analysis provide insights into how well the controller maintains performance in the presence of these challenges.

(iii) Convergence Rate: The speed at which the controller converges to the desired setpoints is a vital aspect of control performance. Convergence indices are used to evaluate the controller's speed of response.

(iv) Simplicity of Implementation**: The ease of implementing the proposed control approach is considered. This aspect is discussed in terms of computational complexity and practical feasibility using OPAL-RT.

Evaluating these performance indices allows for a more detailed and comprehensive analysis of the presented results. It provides a clearer understanding of the controller's strengths in terms of speed tracking, reactive power optimization, disturbance rejection, and robustness against parameter uncertainties, ultimately affirming its suitability for a wide range of practical motor control applications. The simulation results provide clear evidence of the controller's robustness, demonstrating its ability to handle parameter modifications and changes in load torque. The proposed control approach exhibits quick convergence, high stability, and minimal tracking errors while remaining simple to implement.

Data Availability

No data were available for this research work.

Conflicts of Interest

The authors declare that there are no conflicts of interest.

Authors' Contributions

Hafidh Djouadi conceptualized the study, proposed the methodology, provided the software, and wrote the original draft of the manuscript. Kamel Ouari and Houcine Lehouche curated the data and wrote the original draft of the manuscript. Youcef Belkhier curated the data, wrote the original draft of the manuscript, and proposed the methodology.

References

[1] Y. Belkhier, A. Achour, M. Bures et al., "Interconnection and damping assignment passivity-based non-linear observer control for efficiency maximization of permanent magnet synchronous motor," *Energy Reports*, vol. 8, pp. 1350–1361, 2022.

[2] G. Hong, T. Wei, and X. Ding, "Multi-objective optimal design of permanent magnet synchronous motor for high efficiency and high dynamic performance," *IEEE Access*, vol. 6, pp. 23568–23581, 2018.

[3] H. Bouzeria, C. Fetha, T. Bahi, I. Abadlia, Z. Layate, and S. Lekhchine, "Fuzzy logic space vector direct torque control of PMSM for photovoltaic water pumping system," *Energy Procedia*, vol. 74, pp. 760–771, 2015.

[4] K. Urbanski and D. Janiszewski, "Sensorless control of the permanent magnet synchronous motor," *Sensors*, vol. 19, no. 16, p. 3546, 2019.

[5] Y. Li, C. Zhao, Y. Zhou, and Y. Qin, "Model predictive torque control of PMSM based on data drive," *Energy Reports*, vol. 6, pp. 1370–1376, 2020.

[6] A. Apte, V. A. Joshi, H. Mehta, and R. Walambe, "Disturbance-observer-based sensorless control of PMSM using integral state feedback controller," *IEEE Transactions on Power Electronics*, vol. 35, no. 6, pp. 6082–6090, 2020.

[7] G. Scarcella, G. Scelba, M. Pulvirenti, and R. D. Lorenz, "Fault-tolerant capability of deadbeat-direct torque and flux control for three-phase PMSM drives," *IEEE Transactions on Industry Applications*, vol. 53, no. 6, pp. 5496–5508, 2017.

[8] A. A. Alfehaid, E. G. Strangas, and H. K. Khalil, "Speed control of permanent magnet synchronous motor with uncertain parameters and unknown disturbance," *IEEE Transactions on Control Systems Technology*, vol. 29, no. 6, pp. 2639–2646, 2021.

[9] V. Šmídl, Š. Janouš, L. Adam, and Z. Peroutka, "Direct speed control of a PMSM drive using SDRE and convex constrained optimization," *IEEE Transactions on Industrial Electronics*, vol. 65, no. 1, pp. 532–542, 2018.

[10] W. Xu, A. K. Junejo, Y. Liu, M. G. Hussien, and J. Zhu, "An efficient antidisturbance sliding-mode speed control method for PMSM drive systems," *IEEE Transactions on Power Electronics*, vol. 36, no. 6, pp. 6879–6891, 2021.

[11] W. Xu, Y. Jiang, C. Mu, and F. Blaabjerg, "Improved nonlinear flux observer-based second-order SOIFO for PMSM sensorless control," *IEEE Transactions on Power Electronics*, vol. 34, no. 1, pp. 565–579, 2019.

[12] P. Mani, R. Rajan, L. Shanmugam, and Y. H. Joo, "Adaptive fractional fuzzy integral sliding mode control for PMSM model," *IEEE Transactions on Fuzzy Systems*, vol. 27, no. 8, pp. 1674–1686, 2019.

[13] A. K. Junejo, W. Xu, C. Mu, M. M. Ismail, and Y. Liu, "Adaptive speed control of PMSM drive system based a new sliding-mode reaching law," *IEEE Transactions on Power Electronics*, vol. 35, no. 11, pp. 12110–12121, 2020.

[14] A. T. Nguyen, B. A. Basit, H. H. Choi, and J. W. Jung, "Disturbance attenuation for surface-mounted PMSM drives using nonlinear disturbance observer-based sliding mode control," *IEEE Access*, vol. 8, pp. 86345–86356, 2020.

[15] A. Y. Achour, B. Mendil, S. Bacha, and I. Munteanu, "Passivity-based current controller design for a permanent-magnet synchronous motor," *ISA Transactions*, vol. 48, no. 3, pp. 336–346, 2009.

[16] Y. Belkhier and A. Achour, "Passivity-based voltage controller for tidal energy conversion system with permanent magnet synchronous generator," *International Journal of Control, Automation and Systems*, vol. 19, no. 2, pp. 988–998, 2021.

[17] Y. Belkhier, R. N. Shaw, M. Bures et al., "Robust interconnection and damping assignment energy-based control for a permanent magnet synchronous motor using high order sliding mode approach and nonlinear observer," *Energy Reports*, vol. 8, pp. 1731–1740, 2022.

[18] T. H. Nguyen, T. T. Nguyen, K. Minh Le, H. N. Tran, and J. W. Jeon, "An adaptive backstepping sliding-mode control for improving position tracking of a permanent-magnet synchronous motor with a nonlinear disturbance observer," *IEEE Access*, vol. 11, pp. 19173–19185, 2023.

[19] S. Wang, D. Ding, G. Zhang et al., "Flux observer based on enhanced second-order generalized integrator with limit cycle oscillator for sensorless PMSM drives," *IEEE Transactions on Power Electronics*, vol. 38, no. 12, pp. 15982–15995, 2023.

[20] T. Türker, U. Buyukkeles, and A. F. Bakan, "A robust predictive current controller for PMSM drives," *IEEE Transactions on Industrial Electronics*, vol. 63, no. 6, pp. 3906–3914, 2016.

[21] K. C. Kim, "A novel method for minimization of cogging torque and torque ripple for interior permanent magnet synchronous motor," *IEEE Transactions on Magnetics*, vol. 50, no. 2, pp. 793–796, 2014.

[22] A. Mora, A. Orellana, J. Juliet, and R. Cardenas, "Model predictive torque control for torque ripple compensation in variable-speed PMSMs," *IEEE Transactions on Industrial Electronics*, vol. 63, no. 7, pp. 4584–4592, 2016.

[23] H. Tiegna, Y. Amara, and G. Barakat, "Study of cogging torque in axial flux permanent magnet machines using an analytical model," *IEEE Transactions on Magnetics*, vol. 50, no. 2, pp. 845–848, 2014.

[24] S. Chai, L. Wang, and E. Rogers, "A cascade MPC control structure for a PMSM with speed ripple minimization," *IEEE Transactions on Industrial Electronics*, vol. 60, no. 8, pp. 2978–2987, 2013.

[25] S. Wang, C. Xia, X. Gu, and W. Chen, "A novel FCS-model predictive control algorithm with duty cycle optimization for surface-mounted PMSM," 2014.

[26] Y. Zhang and S. Gao, "Simultaneous optimization of voltage vector and duty cycle in model predictive torque control of PMSM drives," in *2014 17th International Conference on Electrical Machines and Systems (ICEMS)*, pp. 3338–3344, IEEE, Hangzhou, China, October 2014.

[27] Z. Ma, S. Saeidi, and R. Kennel, "FPGA implementation of model predictive control with constant switching frequency for PMSM drives," *IEEE Transactions on Industrial Informatics*, vol. 10, no. 4, pp. 2055–2063, 2014.

[28] H. Liu and S. Li, "Speed control for PMSM servo system using predictive functional control and extended state observer," *IEEE Transactions on Industrial Electronics*, vol. 59, no. 2, pp. 1171–1183, 2012.

[29] K. Ouari, Y. Belkhier, H. Djouadi et al., "Improved nonlinear generalized model predictive control for robustness and power enhancement of a DFIG-based wind energy converter," *Frontiers in Energy Research*, vol. 10, Article ID 996206, 2022.

[30] R. Errouissi, A. Al-Durra, S. M. Muyeen, and S. Leng, "Continuous-time model predictive control of a permanent magnet synchronous motor drive with disturbance decoupling," *IET Electric Power Applications*, vol. 11, no. 5, pp. 697–706, 2017.

[31] J. Liu, H. Li, and Y. Deng, "Torque ripple minimization of PMSM based on robust ILC via adaptive sliding mode control," *IEEE Transactions on Power Electronics*, vol. 33, no. 4, pp. 3655–3671, 2018.

[32] A. Isidori, "Nonlinear control system," in *An Introduction*, Springer-Verlag, New York, NY, USA, 3rd edition, 1995.

[33] S. Sriprang, B. Nahid-Mobarakeh, N. Takorabet et al., "Permanent magnet synchronous motor dynamic modeling with state observer-based parameter estimation for AC servomotor drive application," *Applied Science and Engineering Progress*, vol. 12, no. 4, pp. 286–297, 2019.

[34] Y. Zhang, C. Zhao, B. Dai, and Z. Li, "Dynamic simulation of permanent magnet synchronous motor (PMSM) electric vehicle based on Simulink," *Energies*, vol. 15, no. 3, p. 1134, 2022.

[35] K. Ouari, T. Rekioua, and M. Ouhrouche, "Real time simulation of nonlinear generalized predictive control for wind energy conversion system with nonlinear observer," *ISA Transactions*, vol. 53, no. 1, pp. 76–84, 2014.

[36] Y. Belkhier, A. Achour, R. N. Shaw, N. Ullah, M. S. Chowdhury, and K. Techato, "Fuzzy supervisory passivity-based high order-sliding mode control approach for tidal turbine-based permanent magnet synchronous generator conversion system," in *Actuators*, vol. 10, no. 5, p. 92, MDPI, Basel, Switzerland, 2021.

[37] F. Wang, D. Ke, X. Yu, and D. Huang, "Enhanced predictive model based deadbeat control for PMSM drives using exponential extended state observer," *IEEE Transactions on Industrial Electronics*, vol. 69, no. 3, pp. 2357–2369, 2022.

[38] J. Peng and M. Yao, "Overview of predictive control technology for permanent magnet synchronous motor systems," *Applied Sciences*, vol. 13, no. 10, p. 6255, 2023.

[39] M. F. Elmorshedy, W. Xu, F. F. El-Sousy, M. R. Islam, and A. A. Ahmed, "Recent achievements in model predictive control techniques for industrial motor: a comprehensive state-of-the-art," *IEEE Access*, vol. 9, pp. 58170–58191, 2021.

[40] J. Hang, H. Wu, J. Zhang, S. Ding, Y. Huang, and W. Hua, "Cost function-based open-phase fault diagnosis for PMSM drive system with model predictive current control," *IEEE Transactions on Power Electronics*, vol. 36, no. 3, pp. 2574–2583, 2021.

[41] A. Oubelaid, N. Khosravi, Y. Belkhier, N. Taib, and T. Rekioua, "Health-conscious energy management strategy for battery/fuel cell electric vehicles considering power sources dynamics," *Journal of Energy Storage*, vol. 68, Article ID 107676, 2023.

[42] E. Buraimoh and I. E. Davidson, "Laboratory procedure for real-time simulation experiment of renewable energy systems on OPAL-RT digital simulator," in *2022 10th International Conference on Smart Grid (icSmartGrid)*, pp. 221–226, IEEE, Istanbul, Turkey, June 2022.